Proceedings of the 8th International Conference on Gas Hydrates (ICGH8-2014),
Beijing, China, 28 July - 1 August, 2014

EXPERIMENTAL INVESTIGATION OF WATER PERMEABILITY IN QUARTZ SAND AS FUNCTION OF CH_4-HYDRATE SATURATION

Elke KOSSEL, Christian DEUSNER, Nikolaus BIGALKE, Matthias HAECKEL*
GEOMAR Helmholtz Centre for Ocean Research Kiel, Wischhofstr. 1-3, 24148 Kiel, GERMANY

ABSTRACT

Water permeability in gas hydrate bearing sediments is a crucial parameter for the prediction of gas production scenarios. So far, the commonly used permeability models are backed by very few experimental data. Furthermore, detailed knowledge of the exact formation mechanism leads to severe uncertainties in the interpretation of the experimental data. We formed CH_4 hydrates from a methane saturated water solution and used Magnetic Resonance Imaging (MRI) to measure time resolved maps of the three-dimensional gas hydrate saturation. These maps were used for 3D Finite Elements Method (FEM) simulations. The simulation results enabled us to optimize existing models for permeabilities as function of gas hydrate saturation.

Keywords: methane hydrate, hydrate saturation, permeability, MRI, FEM simulations

INTRODUCTION

In times of declining conventional oil and gas resources, the development of unconventional energy resources is becoming more and more attractive [1]. Marine gas hydrates are believed to store vast amounts of natural gas [2-3], but a commercial exploitation of these reservoirs has not yet been established. A crucial factor for the estimation of the productivity and cost effectiveness of natural gas production from marine gas hydrate deposits is the knowledge of the sediment permeability. However, it is not well understood how the formation or dissociation of gas hydrates in the pore space of the marine sediment alters the permeability and consequently the flow characteristics of the involved phases. The objective of this paper is to optimize an equation for water permeability in gas hydrate-bearing quartz sand based on spatially resolved measurements of methane hydrate saturations.

Permeability models

A number of different permeability models have been introduced to and used by the gas hydrate community. Kleinberg et al. provide a summary of models that are based on basic geometric considerations [4]. They include parallel capillary models and grain pack models where the fluid transport is obstructed by wall coating or center occupying solid gas hydrates.

Numerical reservoir simulators tend to use more complex models that include formulations for relative water and gas permeabilities in the presence of gas hydrate. Commonly used equations are the van Genuchten/Mualem model [5-7] and the modified Stone model [8-9]. In contrast to the basic geometry models, they comprise additional parameters which need to be obtained from experimental data. A very popular model for water permeability is an equation that has been introduced by Masuda et al. [10]. It is a simplified form of the modified Stone model with the critical porosity set to zero.

Other models have been obtained from the fit of suitable mathematical functions to experimental

* Corresponding author: Phone: +49 431 600 2123 Fax +49 431 600 2928 E-mail: mhaeckel@geomar.de

data [11-13]. None of these models has experienced a prevalent use.

Published experimental data

Very few experimental data for permeabilities in CH_4-hydrate bearing sediments have been published [4] [11-20]. Most authors have formed gas hydrates by pressurizing moist sediments with a CH_4 atmosphere. The gas hydrate saturation was then calculated from mass balancing. The drawback of this method is that the water distribution in the sample can be homogeneous for relatively small water contents, only. As soon as gravitational forces exceed capillary forces, water will collect at the bottom of the sediment column. Furthermore, at small water saturations, the water forms a wetting film around the sediment grains. This leads to the formation of grain coating gas hydrates while natural gas hydrates are believed to be pore filling [21]. An exception is the work of Kleinberg et al. [4] and Johnson et al. [17], who let methane gas bubble through water saturated sediments.

Ensuring a homogeneous gas hydrate saturation is a crucial factor for the interpretation of the experimental data. Some experimental set-ups did include imaging techniques for a spatially resolved measurement of the gas hydrate distribution. Computed Tomography (CT) imaging was used by [12] [15] [18-19]. Kneafsey and coworkers [9] measured sample profiles with Magnetic Resonance Imaging (MRI). The results of Seol et al. [12] reveal a spatial variation of the gas hydrate saturation, thus contradicting the general assumption of a homogeneous formation.

The measurement of gas permeability is relatively simple compared to the measurement of water permeability: While the gas flow does not change the sample composition of dry samples on the short term, water flow leads to dissolution of the gas hydrates. The water phase is undersaturated with respect to methane and dissolves methane from the hydrate phase. Therefore, gas hydrate saturation is decreasing during permeability measurements with pure water [14-18] [20]. To avoid this effect, Seol et al. [12] used water with dissolved methane for their experiments. The methane concentration has to be subject to a fine balancing since new CH_4-hydrate can form if the concentration of the gas in the liquid phase is too high.

In order to meet the aforementioned experimental difficulties, we created an experimental set-up that allowed us to form gas hydrates from a CH_4-saturated water phase while monitoring the 3-dimensional gas hydrate saturation with MRI. Data evaluation was done by a full 3D Finite Element Method (FEM) simulation that did account for the spatially inhomogeneous formation of gas hydrate.

EXPERIMENTAL PROCEDURE AND DATA EVALUATION

Sample preparation

Quartz sand (G20TEAS, Schlingmeier, Schwülper, Germany) with a mean grain size of 0.29 mm was packed into a sapphire tube and compacted by vibrations. The sapphire tube had a diameter of 1.2 cm and a length of 12 cm. Deionized water was soaked into the tube by a vacuum pump. The water saturated sample was mounted inside an NMR spectrometer (400 MHz Avance III, Bruker Biospin, Rheinstetten, Germany) [22]. Water pressure was then increased to 12 MPa and the sample temperature was set to 5°C. The porosity of the sand sample was 0.35 and the independently measured initial permeability was found to be 35 Darcy.

Deionized water was exposed to a methane atmosphere of 12 MPa at room temperature. The stirred system was allowed to equilibrate for more than 24 hours, resulting in a methane saturated water solution. A MATLAB (The Mathworks, Natick, USA) routine [23] was used to calculate the methane concentration at the relevant thermodynamic conditions [24]. It is 0.123 mol/kg at 22°C and 12 MPa and 0.165 mol/kg at 5°C and 12 MPa. In the presence of gas hydrates, the solubility at 5 °C and 12 MPa reduces to 0.077 mol/kg [25]. The methane saturated water was pumped through the sample from bottom to top at a constant volume flow rate of 0.75 ml/min. Pressure was recorded upstream and downstream of the sample cell. The experiment was automatically terminated when the pressure increase due to gas hydrate formation resulted in upstream pressures above 150 MPa.

Magnetic Resonance Imaging

With our imaging set-up it is not possible to image the full length of the sample tube (12 cm).

Therefore, a stepping motor was used to reposition the sample between measurements. A series of 3D spin echo images, that cover the entire sample, was measured before starting the flow and after the termination of the flow. The image series were merged with a MATLAB code and used for the calculation of the gas hydrate saturation in the sample at the end of the experiment. MRI is only sensitive to the water signal, resulting in a signal loss during gas hydrate formation. Gas hydrate saturation S_H can therefore be calculated from the relative signal difference between a reference image I_0 and an image I of the hydrate-bearing sample:

$$S_H = \frac{I_0 - I}{I_0} \quad (1)$$

Imaging of the full sample during the dynamic process of gas hydrate formation would have resulted in an insufficient time resolution. During the flow of the CH_4-saturated water, only the bottom part of the sample was continuously imaged. The image resolution was 0.9 x 1 x 0.4 mm^3 and the time resolution was 2.3 minutes. The images were used to calculate gas hydrate saturation maps according to eq. (1). We chose to monitor the bottom part because the gas hydrate nucleates stochastically at an unknown position in the sample and grows in upstream direction. When the front reaches the hydrate phase boundary close to the heated fluid inflow, it stops growing and accumulates until the permeability becomes low enough to trigger the termination condition of the experiment. The complete map of the gas hydrate saturation was used to verify that there was no additional massive gas hydrate accumulation further upstream that could have changed the total permeability during the final stages of the experiment.

Finite Element Method Simulations

FEM simulations were performed with the subsurface flow module of the software package COMSOL multiphysics (COMSOL, Palo Alto, USA). The last 9 gas hydrate saturation maps that had been measured before the termination of the experiment were imported as interpolation files. Special care was taken to ensure that the COMSOL interpolation process did not change the characteristics of the measured distribution. Two different permeability models were used for the calculations: The modified model of Stone [8]

$$k = k_0 \left(\frac{\phi - \phi_c}{\phi_0 - \phi_c} \right)^n \quad (2)$$

and the Mualem/van Genuchten model [5-6]

$$k = k_0 \sqrt{\overline{S_W}} \left(1 - \left(1 - \overline{S_W}^{\frac{1}{n}} \right)^n \right)^2 \quad (3)$$

with

$$\overline{S_W} = \frac{S_W - S_R}{1 - S_R} \quad (4)$$

In these equations, k denotes the permeability, k_0 the permeability of the gas hydrate-free sediment, ϕ the porosity, ϕ_c a critical porosity, S_W the water saturation, S_R a residual water saturation and n an unknown exponent. The parameters ϕ_c, S_R and n were varied according to table 1. The output of the simulations was the pressure difference Δp across the modeled sample section.

n	ϕ_c	S_R
5-13 (mod. Stone) 1-5 (Mualem)	0, 0.01	0 ,0.03

Table 1 Parameter variations in FEM simulations

n was varied in steps of 1. A 7th order polynomial (modified Stone model) or a 5th order polynomial (Mualem model) as function of n was fit to the modeled pressure differences to get interpolated results for Δp with steps of 0.1 in n.

The experimentally measured pressure difference was influenced not only by the sediment, but also by elements of the flow system like connectors or filters. Therefore it did not make sense to evaluate absolute values for Δp. Instead, we investigated the change in Δp over time, $\Delta(\Delta p)$, because that change was entirely caused by the gas hydrate formation. For each value of ϕ_c and S_R, the number of n with the smallest quadratic deviation between

experimental data and numerical simulations was determined.

RESULTS AND DISCUSSION

CH_4 hydrate saturation

Figure 1 shows the measured gas hydrate saturation at the end of the experiment. It can be clearly seen that the saturation is not spatially homogeneous. While the saturation reaches local values of up to 0.9, transport will spread to locations with smaller hydrate saturation. This image demonstrates that a full 3-dimensional evaluation of the data is mandatory to obtain reliable results.

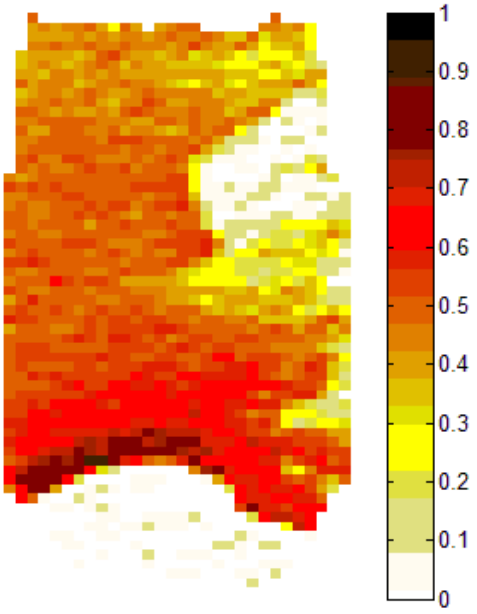

Figure 1 Map of final gas hydrate saturation: central slice of sample, resolution: 0.9 x 0.4 mm^2

Model parameters

The values for the parameter *n* that resulted in the best match between experimental data and simulated results are listed in table 2.

modified Stone		**Mualem**	
$\phi_{c=0}$	$\phi_{c=0.01}$	$S_{R=0}$	$S_{R=0.03}$
11.7	11.1	4.1	4.0

Table 2 Derived values for model exponent *n*

Figure 2 shows the corresponding model graphs for the change in Δp ($\Delta(\Delta p)$) compared to the measured change during the final stage of the experiment. It can be seen that the modified Stone model matches the experimental data better than the Mualem model. The match for the modified Stone model is comparable for both critical porosities. The introduction of a finite value for ϕ_c is balanced by a smaller value for *n*. If the critical porosity equals zero, the modified Stone equation reduces to Masuda's model with *n*=11.7

$$k = k_0 \left(1 - S_H\right)^{11.7} \qquad (5)$$

The value of 11.7 is larger than the results of Minagawa et al. [14] and Konno et al. [19] who report exponents in the range of 8-10 for water permeability in gas hydrate bearing sands. This deviation is plausible because in contrast to the other studies, we evaluated 3D maps of the gas hydrate saturation. We could identify transport pathways with lower than average gas hydrate saturations. A smaller S_H requires a larger *n* to yield the same value for *k*.

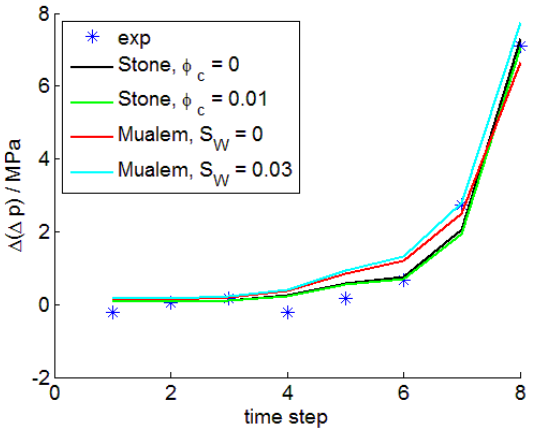

Figure 2 Best match between experimental change in pressure difference and numerical simulation for different permeability models

Figure 3 shows the water permeability as function of gas hydrate saturation for both variations of the modified Stone model. The graphs deviate mainly for high gas hydrate saturations. Since transport in the sample can spread around the highly saturated regions, their influence on the model results was negligible. Therefore, this part of the curve has to be considered as less accurate.

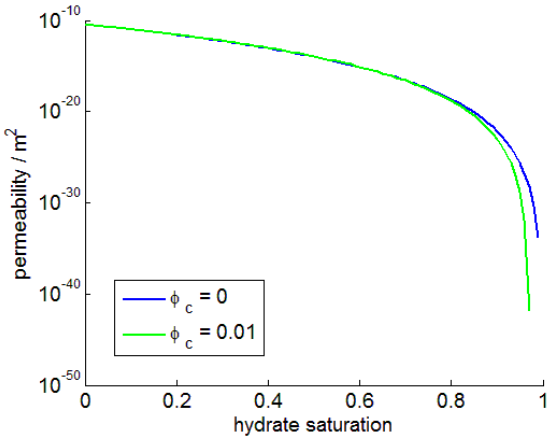

Figure 3 Permeability as function of gas hydrate saturation for the best match of the modified Stone model

CONCLUSIONS

We designed an experimental set-up that enabled us to measure the water permeability in CH_4 hydrate bearing quartz sand in a very controlled way. Gas hydrates were formed from a methane saturated water solution, thus avoiding a possible crossover between grain coating and pore filling behavior. We could measure the spatially resolved gas hydrate distribution and therefore monitor the gas hydrate formation over time. The spatially inhomogeneous hydrate formation required 3D modeling of the fluid flow. We compared two permeability models: The modified Stone model and the Mualem/van Genuchten model. The modified Stone model resulted in a better match with the experimental data. The introduction of a finite critical porosity did not improve the match. We derived higher model exponents than other studies, which can be explained by our more detailed knowledge of the gas hydrate saturation: We could identify pathways with smaller than average gas hydrate saturation that dominated the transport and required a higher value for the exponent *n*.

ACKNOWLEDGEMENTS

This research was funded by the German Ministry of Economy (BMWi) through the SUGAR project (grant No. 03SX320A).

REFERENCES

[1] Rogner HH. *An assessment of world hydrocarbon resources*. Annu Rev Energ Environ. 1997;22(:217-62.

[2] Wallmann K, Pinero E, Burwicz E, Haeckel M, Hensen C, Dale A, et al. *The Global Inventory of Methane Hydrate in Marine Sediments: A Theoretical Approach*. Energies 2012;5(7):2449-98.

[3] Pinero E, Marquardt M, Hensen C, Haeckel M, Wallmann K. *Estimation of the global inventory of methane hydrates in marine sediments using transfer functions*. Biogeosciences 2013;10(2):959-75.

[4] Kleinberg RL, Flaum C, Griffin DD, Brewer PG, Malby GE, Peltzer ET, et al. *Deep sea NMR: Methane hydrate growth habit in porous media and its relationship to hydraulic permeability, deposit accumulation, and submarine slope stability*. J Geophys Res-Solid Earth 2003;108(B10):12 1-17.

[5] Mualem Y. *A new model for predicting the hydraulic conductivity of unsaturated porous media.* Water Resources Research 1976;12(3):513-22.

[6] van Genuchten MT. *A closed-form equation for predicting the hydraulic conductivity of unsaturated soils*. Soil Science Society of America Journal 1980;44(5):892-8.

[7] Moridis GJ, Collett TS, Dallimore SR, Inoue T, Mroz T. *Analysis and interpretation of the thermal test of gas hydrate dissociation in the JAPEX/JNOC/GSC et al. Mallik 5L-38 gas hydrate production research well*. Geological Survey of Canada Bulletin. 2005;585:1-21.

[8] Stone HL. *Probability model for estimating three-phase relative permeability*. Journal of Petroleum Technology 1970;22(2):214-8.

[9] Schroderbek D, Farrell H, Hester K, Howard J, Raterman K, Silpngarmlert S, et al. *ConocoPhillips gas hydrate production test final technical report*. DOE Report 2013.

[10] Masuda Y, Naganawa S, Ando S, Sato K. *Numerical calculations of gas hydrate production performance from reservoirs containing natural gas hydrates.* Proceedings Western Regional Meeting, Society of Petroleum Engineers. Long Beach, California1997.

[11] Kurihara M, Ouchi H, Inoue T, Yonezawa T, Masuda Y, Dallimore SR, et al. *Analysis of the JAPEX/JNOC/GSC et al. Mallik 5L-38 gas hydrate thermal-production test through numerical simulation*. Geological Survey of

Canada Bulletin. 2005;585:1-20.
[12] Seol Y, Kneafsey TJ. *Methane hydrate induced permeability modification for multiphase flow in unsaturated porous media*. J Geophys Res-Solid Earth 2011;116(B08102):1-15.
[13] Delli ML, Grozic JLH. *Prediction Performance of Permeability Models in Gas-Hydrate-Bearing Sands*. SPE J 2013;18(2):274-84.
[14] Minagawa H, Ohmura R, Kamata Y, Ebinuma T, Narita H. *Water permeability measurements of gas hydrate-bearing sediments*. *In: Proceedings of the Fith International Conference on Gas Hydrates. Trondheim, Norway*2005.
[15] Jin Y, Hayashi J, Nagao J, Suzuki K, Minagawa H, Ebinuma T, et al. *New method of assessing absolute permeability of natural methane hydrate sediments by microfocus X-ray computed tomography*. Jpn J Appl Phys Part 1 - Regul Pap Brief Commun Rev Pap 2007;46(5A):3159-62.
[16] Sakamoto Y, Komai T, Myazaki K, Tenma N, Yamaguchi T, Zyvoloski G. *Laboratory-scale experiments of methane hydrate dissociation process in a porous media and numerical study for the estimation of permeability in methane hydrate reservoir*. Journal of Thermodynamic. 2010;2010:1-13.
[17] Johnson A, Patil S, Dandekar A. *Experimental investigation of gas-water relative permeability for gas-hydrate-bearing sediments from the Mount Elbert Gas Hydrate Stratigraphic Test Well, Alaska North Slope* Mar Pet Geol. 2011;28(2):419-26.
[18] Kneafsey TJ, Seol Y, Gupta A, Tomutsa L. *Permeability of Laboratory-Formed Methane-Hydrate-Bearing Sand: Measurements and Observations Using X-Ray Computed Tomography*. SPE J 2011;16(1):78-94.
[19] Konno Y, Jin Y, Uchiumi T, Nagao J. *Multiple-pressure-tapped core holder combined with X-ray computed tomography scanning for gas-water permeability measurements of methane-hydrate-bearing sediments*. Rev Sci Instrum 2013;84(064501):1-5.
[20] Li B, Li XS, Li G, Jia JL, Feng JC. *Measurements of Water Permeability in Unconsolidated Porous Media with Methane Hydrate Formation*. In: Proceedings Western Regional Meeting, Society of Petroleum Engineers, Long Beach, California, 1997.
[21] Waite WF, Santamarina JC, Cortes DD, Dugan B, Espinoza DN, Germaine J, et al. *Physical properties of hydrate-bearing sediments. Reviews of Geophysics* 2009;47.
[22] Kossel E, Deusner C, Bigalke N, Haeckel M. *Magnetic Resonance Imaging of Gas Hydrate Formation and Conversion at Sub-Seafloor Conditions*. Diffusion Fundamentals. 2013;18(15):1-4.
[23] Kossel E, Bigalke N, Pinero E, Haeckel M. *The SUGAR Toolbox : a library of numerical algorithms and data for modelling of gas hydrate systems and marine environments*. GEOMAR Report. Kiel: GEOMAR Helmholtz-Zentrum für Ozeanforschung Kiel; 2013.
[24] Duan ZH, Mao SD. *A thermodynamic model for calculating methane solubility, density and gas phase composition of methane-bearing aqueous fluids from 273 to 523 K and from 1 to 2000 bar*. Geochimica et Cosmochimica Acta 2006;70(13):3369-86.
[25] Tishchenko P, Hensen C, Wallmann K, Wong CS. *Calculation of the stability and solubility of methane hydrate in seawater*. Chemical Geology. 2005;219:37-52.